Title
Lithium isotope fractionation during uptake by gibbsite

Authors
Wimpenny, Josh
Colla, Christopher A
Yu, Ping
et al.

Publication Date
2015-11-01

DOI
10.1016/j.gca.2015.07.011

Peer reviewed

Available online at www.sciencedirect.com

ScienceDirect

Geochimica et Cosmochimica Acta 168 (2015) 133–150

Geochimica et Cosmochimica Acta

www.elsevier.com/locate/gca

Lithium isotope fractionation during uptake by gibbsite

Josh Wimpenny [a,*], Christopher A. Colla [a], Ping Yu [b], Qing-Zhu Yin [a], James R. Rustad [a], William H. Casey [a,c]

[a] Department of Earth and Planetary Sciences, University of California, One Shields Avenue, Davis, CA 95616, United States
[b] The Keck NMR Facility, University of California, One Shields Avenue, Davis, CA 95616, United States
[c] Department of Chemistry, University of California, One Shields Avenue, Davis, CA 95616, United States

Received 5 November 2014; accepted in revised form 8 July 2015; available online 15 July 2015

Abstract

The intercalation of lithium from solution into the six-membered μ_2-oxo rings on the basal planes of gibbsite is well-constrained chemically. The product is a lithiated layered-double hydroxide solid that forms via *in situ* phase change. The reaction has well established kinetics and is associated with a distinct swelling of the gibbsite as counter ions enter the interlayer to balance the charge of lithiation. Lithium reacts to fill a fixed and well identifiable crystallographic site and has no solvation waters. Our lithium-isotope data shows that ^{6}Li is favored during this intercalation and that the solid-solution fractionation depends on temperature, electrolyte concentration and counter ion identity (whether Cl^-, NO_3^- or ClO_4^-). We find that the amount of isotopic fractionation between solid and solution ($\Delta Li_{solid\text{-}solution}$) varies with the amount of lithium taken up into the gibbsite structure, which itself depends upon the extent of conversion and also varies with electrolyte concentration and in the counter ion in the order: $ClO_4^- < NO_3^- < Cl^-$. Higher electrolyte concentrations cause more rapid expansion of the gibbsite interlayer and some counter ions, such as Cl^-, are more easily taken up than others, probably because they ease diffusion. The relationship between lithium loading and $\Delta Li_{solid\text{-}solution}$ indicates two stages: (1) uptake into the crystallographic sites that favors light lithium, in parallel with adsorption of solvated cations, and (2) continued uptake of solvated cations after all available octahedral vacancies are filled; this second stage has no isotopic preference. The two-step reaction progress is supported by solid-state NMR spectra that clearly resolve a second reservoir of lithium in addition to the expected layered double-hydroxide phase.

1. INTRODUCTION

Lithium has two isotopes (^{6}Li and ^{7}Li) that have a ~16% difference in mass and so fractionate readily in low-temperature environments. While lithium isotopes are not significantly fractionated during mineral dissolution [e.g. (Pistiner and Henderson, 2003; Wimpenny et al., 2010a; Verney-Carron et al., 2011)] they are highly sensitive to the formation of secondary silicate minerals such as clays that preferentially uptake ^{6}Li leaving the residual lithium in solution enriched in ^{7}Li [e.g. (Brenot et al., 2008; Chan et al., 1992, 1993, 1994; Huh et al., 1998; Pistiner and Henderson, 2003; Rudnick et al., 2004; Kisakurek et al., 2005; Chan and Hein, 2007; Wimpenny et al., 2010a,b; Pogge von Strandmann et al., 2012; Ryu et al., 2014)]. By this mechanism, river waters contain dissolved lithium that is highly isotopically fractionated [δ^7Li + 23‰, (Huh et al., 1998)] relative to bulk silicate earth [δ^7Li + 4‰, (Chan et al., 1992)] and the weathered upper continental crust [δ^7Li 0‰, (Teng et al., 2004)]. This sensitivity of lithium isotopes to secondary mineral formation suggests use as a tracer to infer past changes in continental weathering (Misra and Froelich, 2012; Pogge von Strandmann et al., 2013).

* Corresponding author.
E-mail address: jbwimpenny@ucdavis.edu (J. Wimpenny).

http://dx.doi.org/10.1016/j.gca.2015.07.011
0016-7037/

To exploit the isotope system as a weathering tracer, it is important to understand the mechanisms by which its isotopes become fractionated in clays and to gauge the uncertainties in assigning factors to particular reactions. If the reaction is well constrained structurally, equilibrium fractionation of stable isotopes can be predicted by comparing calculated vibrational energies. The vibrational energy level of a system will be lower for bonds involving heavier isotopes, so at equilibrium the heavier isotope preferentially partitions into the material in which the element is bound most strongly [e.g., (Bigeleisen and Mayer, 1947; Rustad et al., 2010)]. Short bonds tend to be stiffer and stronger than long bonds (Badger, 1934) and metal–oxygen bond lengths decrease with coordination number so lower coordination environments tend to have heavier isotopic signatures.

For example, recent work shows that changes in the Ca(II) coordination number controls Ca-isotope systematics when the solvated ions are incorporated intact into solid structures (Colla et al., 2013). This work remains highly relevant to the Li-isotope system where the lithium aqua ion is thought to exist in coordination geometries ranging from trigonal planar to octahedral (Supplemental Fig. S1), as a function of the activity of water (Richens, 1997). Such changes could directly influence the isotopic fractionation measured between solution and a solid phase.

1.1. Studies of lithium-isotope fractionation

To date, lithium-isotope fractionation has been quantified through a combination of natural and experimental studies using both inorganic solids such as clays and organic exchangers such as crown ethers [e.g. (Heumann, 1985; Nishizawa et al., 1988; Kim et al., 1997), also see Table 1]. The tendency of lithium isotopes to fractionate at low temperature has long been known since early work by Taylor and Urey (1938) showing preferential uptake of ^{6}Li into zeolites with an $\alpha_{solid\text{-}solution}$ (δ^7Li_{solid}-$\delta^7Li_{solution}$) of 0.978. Similar fractionation factors were also estimated from natural studies of lithium in seafloor basalt, Fe-Mn crusts and Fe-oxyhydroxides (Chan et al., 1992; Chan and Hein, 2007; Wimpenny et al., 2010b) and experimental studies determining the fractionation of lithium during uptake into gibbsite, kaolinite, vermiculite, illite and smectite (Brenot et al., 2008; Zhang et al., 1998; Pistiner and Henderson, 2003; Williams and Hervig, 2005). The fractionation factor ($\alpha_{solid\text{-}solution}$) depends on both mineral type and temperature (Brenot et al., 2008; Taylor and Urey,

Table 1
Literature data for lithium-isotope fractionation during uptake into macrocyclic compounds and inorganic exchangers such as clay minerals.

Study	Exchanger	Eluant/solution phase	$\alpha_{solid\text{-}solution}$	Isotope in solid phase	T (°C)
Macrocyclic compounds					
Ban et al. (2002)	Monobenzo-15-crown-5	0.55 M LiCl in methanol, 12 M HCl	0.9873	^{6}Li	35
Kim (2002)	Cyclic N_3O_3 trimerrifield peptide resin (18C6)	4 M NH_4Cl	1.028	^{7}Li	20
Kim et al. (1991)	Monobenzo-15-crown-5	5% H_2O in acetonitrile	0.947	^{6}Li	23
Kim et al. (1995)	Dibenzo pyridino diamide azacrown (DBPDA)	Acetonitrile	0.966	^{6}Li	20
Kim et al. (1997)	Cyclic triazatetramerrifield resin	1 M NH_4Cl	0.932	^{6}Li	20
Kim et al. (1998)	Azacrown tetramerrifield peptide resin	0.5 M NH_4Cl	1.00127	^{7}Li	25
Kim et al. (1998)	NTOE	0.01 M HCl	1.0242	^{7}Li	25
Kim et al. (1999)	N_4O_2 azacrown	0.01 M NH_4Cl	1.038	Unclear	20
Kim et al. (2000)	Amino benzo-15-crown-5	1 M NH_4Cl	1.026	^{7}Li	20
Nishizawa and Watanabe (1986)	Cryptand (2B,2,1)		0.959	^{6}Li	Room temp.
Nishizawa et al. (1984)	Benzo-15-crown-5		0.965–0.998	^{6}Li	Room temp.
Nishizawa et al. (1984)	Cryptand (2B,2,1)	Methanol solution of LiX	0.953–0.965	^{6}Li	
Nishizawa et al. (1988)	Benzo-15-crown-5		0.960–1.000	^{6}Li	20
Ooi et al. (1999)	Ti-phosphate exchanger	0.05 M $(NH_4)_2CO_3$	0.993	^{6}Li	20
Otake et al. (2006)	Phenol type benzo-15-crown-5	Methanol-HCl mix	0.967	^{6}Li	35
Kim et al. (2003)	Aminobenzo-18-crown-6	2 M NH_4Cl	1.0095	^{7}Li	20
Oi et al. (1991)	Cation exchange resin		1.00089–1.00171	^{7}Li	
Inorganic materials					
Pistiner and Henderson (2003)	Gibbsite		0.985	^{6}Li	
Zhang (1998)	Kaolinite and vermiculite		0.972–0.979	^{6}Li	25
Vigier (2008)	Smectite		0.984	^{6}Li	3
Wimpenny (2010)	Fe-oxyhydroxides		0.98	^{6}Li	
Chan and Hein (2007)	Fe-Mn crusts		0.978–0.999	^{6}Li	
Taylor and Urey (1938)	Zeolite		0.978	^{6}Li	

1938; Wunder et al., 2006, 2007). Other controls over $\alpha_{solid\text{-}solution}$ for lithium isotopes are not well constrained by geochemists; the influence of ionic strength and solution composition on α are less intuitive and have been less well characterized. Vigier et al. (2008) investigated lithium concentration (3 M LiCl vs 0.3 M LiCl) at 90 °C and the effect of solution seawater matrix on isotopic fractionation during smectite growth but in all cases they observe no change in $\alpha_{solid\text{-}solution}$.

There exist several often overlooked studies regarding lithium-isotope separation by macrocyclic oxo-ring compounds that stemmed from the use of enriched ^{7}Li (as LiOH) in nuclear-fission reactors [e.g. (Ban et al., 2002)] and ^{6}Li in tritium production. Crown ethers and cryptand resins (Supplemental Fig. S2) preferentially select either ^{6}Li or ^{7}Li from solution, and studies show that the fractionation factor ($\alpha_{solid\text{-}solution}$) associated with this site-specific uptake spans a large range from 0.932 to 1.028 (see Table 1). Of these studies, three by Nishizawa and co-workers are particularly relevant to the present study. The first of these shows that isotopic fractionation of lithium during uptake into cryptand resin varies with temperature, with $\alpha_{solid\text{-}solution}$ decreasing systematically from 0.953 to 0.965 as temperature increases from 0 to 40 °C (Nishizawa et al., 1984a). The second study shows that during uptake of lithium into benzo-15-crown-5 ether the fractionation factor is sensitive to the identity of the counter ion (LiX where X is the counter ion), with the amount of fractionation increasing in the sequence $Cl^- < Br^- < I^-$ (Nishizawa et al., 1984b). Lastly, during reaction of dissolved LiCl with benzo-15-crown-5 ether, it was found that the fractionation factor depends on solution concentration; increasing from ~1 using 2 M LiCl to 0.960 using 10 M LiCl (Nishizawa and Takano, 1988). These results contrast to the results of Vigier et al. (2008), although the experimental conditions used by Vigier and coworkers were very different. The crown-ether work is particularly relevant because these molecules trap Li(I) in an array of five- or six-member rings of μ_2-oxo groups. Similarly, the ring on the basal sheet of gibbsite (Supplemental Fig. S2) also traps Li(I) into a six-membered ring of μ_2-oxo.

In addition to equilibrium fractionation, irreversible kinetic processes and diffusive transport can also fractionate stable isotopes. The diffusion of ^{6}Li is faster than ^{7}Li and this difference can impart important fractionation effects, even at relatively low temperatures. For example, Richter et al. (2006) show that the ^{6}Li diffuses more rapidly than ^{7}Li (by ~3%) when diffusing between two fluid reservoirs at 25 °C. Conceivably the more rapid diffusion of ^{6}Li in water as ions or ion pairs could result in secondary phases such as clays being isotopically lighter than fluid phases such as river water, or experimental solutions, at least prior to the establishment of isotopic equilibrium.

1.2. Li intercalation in gibbsite

We here perform a detailed investigation of how lithium isotopes behave during uptake into the common alteration phase gibbsite, $Al(OH)_3$, where the reaction is particularly well studied. Gibbsite ($Al(OH)_3$) is often viewed as a structural building block for dioctahedral clays and consists of double layers of μ_2-OH separating Al(III) that occupy two-thirds of the interstitial sites within these layers (Saalfeld and Wedde, 1974). Stacked layers are bound to one another by a combination of van der Waals' forces and hydrogen bonds and the basal sheets can be viewed as linked six-membered rings of metals or oxygens (Supplemental Fig. S2). In order to maintain charge balance, there is a vacancy in the six-membered ring and it is in this site that Li(I) reacts preferentially. The tendency for gibbsite to take up Li(I) in the rings is well known (Besserguenev et al., 1997; Isupov et al., 1998; Fogg and O'Hare, 1999; Wang et al., 2007) and is exploited industrially to form the layered-double-hydroxide solid $[LiAl_2(OH)_6]X.nH_2O$ as written in Eq. (1), where X can be Cl, I, Br, or NO_3:

$$LiX(aq) + 2Al(OH)_3(s) \rightarrow [LiAl_2(OH)_6]X \cdot nH_2O(s) \quad (1)$$

This reaction proceeds without dissolution and reprecipitation of the mineral lattice. To maintain a charge balance, gibbsite must also take up the accompanying counter ion (e.g. Cl^-) into the mineral lattice (Besserguenev et al., 1997). Detailed work by O'Hare and coworkers (Fogg and O'Hare, 1999; Williams and O'Hare, 2006) present comprehensive kinetic data and show that the rate of Li(I) intercalation into gibbsite depends on temperature, ionic strength and the counter ion species. The rate-limiting step of Li(I) intercalation appears to be expansion of the interlayer [e.g. (Williams and O'Hare, 2006)]. Once Li(I) and its counter ion are accommodated within the hydroxide layers it is then relatively easy for Li(I) to move rapidly into the layer voids (i.e. the six membered ring in the octahedral sheet). More detailed description of the Li(I)-intercalation mechanism is given in Isupov et al., 1998, and Williams and O'Hare, 2006.

While the structure of gibbsite is well known and intercalation of Li(I) has been well studied (Besserguenev et al., 1997; Isupov et al., 1998; Fogg and O'Hare, 1999; Hou and Kirkpatrick, 2001), measurements of isotopic fractionation between solution and gibbsite is not. To date, only one previous study has investigated lithium-isotope fractionation during uptake into gibbsite (Pistiner and Henderson, 2003) showing that gibbsite preferentially takes up ^{6}Li from solution with a fractionation factor $\alpha_{solid\text{-}solution}$ of 0.986. However, investigating how $\alpha_{solid\text{-}solution}$ might be influenced by parameters such as ionic strength and counter ion identity was not the goal of the study.

Because we employ high electrolyte concentrations in this study, we must also examine the hypothesis that lithium-isotope fractionation is affected by subtle changes in the activity of water that accompany these changes in solution composition. This hypothesis extends directly from previous work where the intercalation of lithium was shown to be sensitive to ionic strength, electrolyte concentration and counter ion identity. To this end we will investigate the intercalation of Li(I) into gibbsite by comparing computational and experimental results. The computational results examine fractionation from reasonable estimates of the structure of the aqueous Li^+ ion. The experimental methods will involve reacting a pure gibbsite solid with solutions of

LiCl, $LiNO_3$, and $LiClO_4$ with concentrations that range from 1 M to 12 M. We understand that these solution compositions are well beyond geochemical conditions but the rate of lithium intercalation into gibbsite is strongly dependent on the molarity of the fluid phase (e.g. Fogg and O'Hare, 1999). To understand how lithium isotopes behave during intercalation, and to investigate site specific isotopic fractionation it is important to vary the extent of reaction. Moreover, to promote intercalation of lithium on an experimental timescale of days to months the kinetic data (Fogg and O'Hare, 1999) showed that relatively concentrated solutions were necessary. Hence, to satisfy these requirements the experiments are performed using a range of relatively concentrated solutions, with full knowledge that these concentrations are not representative of natural systems. Elemental and isotopic analyses of the solid and solution will be characterized by ICP-MS, and these data will be supplemented by SEM images and XRD analyses of the reacted solid. We will also apply solid-state nuclear-magnetic resonance (NMR) techniques in order to characterize the structural changes of gibbsite upon lithiation and the coordination environments of lithium before and after the lithium uptake process. NMR spectroscopy is a powerful tool to probe the local coordination environment of an atom in the crystal structure and is widely used for structural studies of solids by many mineralogists (Kirkpatrick, 1988; Stebbins, 1988; Stebbins and Xue, 2014). Combined, these data will provide us with a detailed understanding of the processes that control lithium intercalation into a layered clay mineral such as gibbsite, and how these processes influence lithium isotope systematics. Characterizing site specific fractionation is crucial for understanding isotopic systematics during mineral–water interactions; hence it is highly relevant to the interpretation of lithium isotope behavior in natural systems such as rivers and seawater.

2. METHODS

2.1. Isotope conventions

The isotopic composition of lithium (δ^7Li) is the measured ratio of its isotopes in a sample normalized to the ratio of its isotopes in a standard, in this case the NIST lithium standard LSVEC:

$$\delta^7Li = \left[\left(\frac{\left(\frac{^7Li}{^6Li}\right)_{sample}}{\left(\frac{^7Li}{^6Li}\right)_{LSVEC}}\right) - 1\right] \times 1000 \quad (2)$$

The lithium-isotope fractionation factor ($\Delta^{7/6}Li_{solid\text{-}solution}$), is the δ^7Li value of the solid minus the δ^7Li value of the solution, given in Eq. (3):

$$\Delta^7Li_{solid\text{-}solution} = \delta^7Li_{solid} - \delta^7Li_{solution} \quad (3)$$

The lithium-isotope fractionation factor ($\Delta^{7/6}Li_{solid\text{-}solution}$) is approximately equal to the alpha fractionation factor ($\alpha_{solid\text{-}solution}$) in Eq. (4):

$$\Delta^7Li_{solid\text{-}solution} \approx 10^3 \ln \alpha_{solid\text{-}solution} \quad (4)$$

2.2. Experiments

We chose experimental conditions that matched the studies of O'Hare (Fogg and O'Hare (1999) and Williams and O'Hare (2006)). Experimental temperatures ranged from ambient to 120 °C, and LiCl, $LiNO_3$ and $LiClO_4$ solutions varied over concentrations ranging from 1 M to 12 M (Table 2). All stock solutions were made and stored in sealed glass volumetric flasks for use in the experiments. In all experiments 1 g of solid powdered gibbsite was added to an ultra-clean beaker and mixed with 10 mL of one of the stock solutions. The pH of all solution-mineral experiments was ambient. The starting mineral reagent gibbsite acquired from Alcoa company was equilibrated in 1 N HCl for 14 days and then rinsed with >18 MΩ H_2O for another 14 days and then oven dried at 100 °C before use [see (Rosenqvist and Casey, 2004)].

Solids and solutions were sampled the first 2 days then every other day for 2 weeks and the solid- and solution-isotopic compositions measured via MC-ICP-MS. Experiments were run at different concentrations depending on the counter ion to Li(I) (Table 2). For example, the LiCl solutions were: 1 M, 4 M, 8 M, and 12 M, and two different temperatures, 25 °C and 120 °C. Solids were separated from solutions via a syringe filter, where the solution-mineral slush was drawn into a 12 mL syringe and then passed through a 0.45 μm synthetic filter. The solutions were slightly acidic ($3.5 < pH < 6$) due to $LiOH^+$ formation and the pH depended upon the total lithium electrolyte added. The values elevated and became very stable pH values upon addition of the gibbsite ($4 < pH < 5.7$), again varying with the total electrolyte concentration.

2.3. SEM and XRD analyses

2.3.1. X-ray Diffraction

Li(I)-intercalation yields a layered double-hydroxide structure of $[LiAl_2(OH)_6]Cl.nH_2O$. The successful characterization of this compound was carried out on a Bruker D8 Advance powder X-ray diffractometer (Bruker AXS Inc.), equipped with a Cu-K_α radiation source with a wavelength of 1.54 Å. The data was collected from 5° to 70° 2θ at 0.02° 2θ per step and a collection time of 0.5 s per step. The solid powdered materials were smeared onto a zero-background sample holder before being mounted onto the diffractometer.

2.3.2. Electron microscopy

Samples were prepared for SEM analysis via syringe filtration. To remove any excess water or salt solution, acetone was passed through the syringe filter and the final products were dried under vacuum for approximately 15 h. All solids were mounted on a pin mount with a small piece of carbon tape. Electron beam power was at 5 kV on a Hitachi High Technologies America, Inc. S-4100 field emission scanning electron microscope.

Table 2
Lithium isotope data for standards and samples from the gibbsite intercalation experiments. Lithium concentration data are also included for solid phases from the experiments performed at 25 °C. All isotope samples were measured three times.

No. of days	Molarity	T (°C)	δ^7Li (solution)	2σ	δ^7Li (solid)	2σ	$\Delta^7Li_{solid\text{-}solution}$	[Li_{solid}] wt%
LiCl experiments								
1	1	25	5.0	0.3	4.1	0.6	−0.9	0.16
2	1	25	5.3	0.1	4.9	0.0	−0.4	0.20
5	1	25	4.1	0.2	6.5	0.4	2.4	0.01
12	1	25	4.6	0.2	4.5	0.2	−0.1	0.08
25	1	25	3.8	0.2	4.9	0.3	1.1	0.10
1	4	25	4.6	0.2	5.6	0.3	1.0	0.83
4	4	25	5.0	0.4	5.1	0.4	0.1	0.75
7	4	25	5.5	0.7	0.9	0.5	−4.6	1.11
23	4	25	5.6	0.2	−2.8	0.2	−8.4	1.77
45	4	25	6.5	0.3	9.7	0.4	16.2	2.19
52	4	25	7.5	0.5	−8.8	0.0	−16.3	2.86
177	4	25	7.2	0.3	−2.7	0.3	−9.9	3.45
1	8	25	4.7	0.3	3.5	0.3	−1.2	1.80
4	8	25	5.8	0.2	−2.2	0.2	−8.0	2.46
7	8	25	6.8	0.2	−2.5	0.3	9.3	
23	8	25	6.8	0.2	−2.5	0.4	−9.4	3.49
45	8	25	6.1	0.2	−7.5	0.4	−13.5	3.50
52	8	25	6.5	0.2	−10.4	0.1	−16.9	3.49
177	8	25	6.3	0.5	−5.8	0.4	−9.9	4.11
1	12	25	5.1	0.4	1.9	0.5	−3.2	3.89
2	12	25	5.6	0.1	0.6	0.1	−5.0	4.09
5	12	25	5.6	0.1	−2.4	0.2	−8.0	3.97
12	12	25	5.3	0.1	−1.9	0.0	−7.2	3.89
25	12	25	5.5	0.4	−1.0	0.4	−6.5	5.06
1	1	120	4.6	0.3	3.0	0.5	−1.5	
2	1	120	4.8	0.1	4.6	0.1	−0.2	
5	1	120	4.8	0.2	4.0	0.5	−0.8	
12	1	120	4.6	0.3	4.8	0.3	0.2	
1	12	120	4.4	0.2	5.1	0.5	0.7	
2	12	120	4.9	0.0	Not measured			
5	12	120	4.8	0.2	4.3	0.0	−0.5	
12	12	120	4.9	0.3	4.8	0.2	−0.1	
$LiClO_4$ experiment								
1	5	25	2.2	0.7	2.4	0.8	0.2	0.16
2	5	25	2.2	0.3	2.2	0.6	0.0	0.51
7	5	25	1.8	0.0	1.8	0.3	0.0	0.10
17	5	25	1.9	0.1	2.3	0.2	0.4	0.05
29	5	25	1.9	0.3	1.8	0.2	−0.1	0.05
35	5	25	2.0	0.1	2.0	0.3	0.1	0.07
$LiNO_3$ experiments								
1	1	25	6.4	0.7	6.1	0.4	−0.3	0.21
2	1	25	6.6	0.4	5.8	0.2	−0.8	0.04
5	1	25	6.7	0.4	6.3	0.1	−0.4	0.09
26	1	25	6.4	0.1	6.3	0.3	−0.1	0.17
1	4	25	5.7	0.4	5.3	0.0	−0.5	0.08
2	4	25	5.9	0.2	6.3	0.1	0.3	0.12
5	4	25	6.0	0.2	6.1	0.4	0.2	0.40
26	4	25	6.2	0.2	2.1	0.4	−4.1	0.29
33	4	25	6.1	0.4	1.8	0.2	−4.3	

Standards	δ^7Li	2sd	n
Specpure Li	104.5	0.7	24
LSVEC (Col.)	0.1	0.6	13
LiCl	4.6	0.2	6
$LiClO_4$	2.1	0.3	3
$LiNO_3$	6.5	0.3	3

2.3.3. Nuclear magnetic resonance (NMR) spectroscopy

All solid-state magic-angle-spinning (MAS) NMR spectra were collected on a Bruker AVANCE 500 MHz spectrometer equipped with an 11.74 T magnet, using a Bruker 4 mm MAS triple-resonance probe. All samples were loaded into 4 mm zirconia rotors and spun at 12 kHz. For ^{7}Li NMR experiments a typical 30° pulse and recycle delay time of 5 s were used. The ^{7}Li chemical shift was externally referenced to 1 M LiCl solution. For ^{27}Al NMR experiments, the pulse length was 0.35 μs (corresponding to 30 degree tip angle), and the recycle delay was 0.5 s. The ^{27}Al chemical shift was externally referenced to 1 M $AlCl_3$ solution. ^{7}Li was chosen as the target nucleus because it is quadrupolar, has 92.41% natural abundance and resonates at 194.36 MHz. All fits to the NMR spectra were made using the program DMFIT (Massiot et al., 2002).

2.4. Isotopic analyses

Gibbsite samples were dissolved using a 1:1 mixture of concentrated HNO_3 and HCl, and heating at 120 °C for 24 h, after which no solid residue was present. This solution was then evaporated to dryness and the residue redissolved in 0.2 N HCl for processing through cation columns. Small aliquots of solution samples were also dried down and redissolved in 0.2 N HCl. All samples were separated from potential matrix species using a column procedure adapted from James & Palmer (2000). Savillex columns with dimensions of 0.8 cm by 10 cm were filled with Biorad AG50-X8 resin to a height of 8.5 cm (measured in 0.2 N HCl). These columns were previously calibrated to ensure a 100% yield of lithium, and a good separation between lithium and sodium. The sample matrix used in this study is quite unlike typical rocks or water samples, being highly enriched in lithium relative to other cations, with no sodium present, so to ensure that the column chemistry was calibrated correctly we routinely processed the pure lithium LSVEC standard through the columns and measured its isotopic composition relative to unprocessed LSVEC (see below for more details). Samples were loaded, eluted and collected in 0.2 N HCl. Collected samples were dried down and redissolved in concentrated HNO_3 in order to oxidize any organics that were derived from the resin. Upon drying again, these samples were diluted in 1 ml of 2% HNO_3 ready for analysis by multi-collector ICP-MS.

All samples were analyzed using a Thermo-Scientific Neptune Plus at UC Davis. The Neptune was set up with a high sensitivity 'x' skimmer cone and a standard sampling cone. Samples and standards were introduced to the plasma via an Apex IR which partially desolvates the sample. As there are no interferences to worry about for lithium, the analyses were all performed at low resolution. In general 10 ppb of lithium gave a signal intensity of ~10 V ^{7}Li and the 2% HNO_3 running blank was less than 50 mV (i.e. a signal to blank ratio of 200) using 10^{11} ohm resistors and a Teflon nebulizer with an uptake rate of 50 μl/min. The two isotopes of lithium were measured on the L4 and H4 Faraday collectors with a dummy mass on the center cup. Measured ratios must be normalized to a standard in order to correct for mass bias effects; following the convention in lithium-isotope studies all samples were bracketed by the LSVEC lithium carbonate standard. To assess the accuracy of our analyses, and long term precision we measured several LSVEC samples that had been processed through chemistry. On average these standards gave a δ^{7}Li value of $0.1 \pm 0.6‰$ ($n = 13$). We also routinely measured an in-house standard of pure lithium (Alfa Aesar Specpure Li) during every analytical session, with a δ^{7}Li value of $104.5 \pm 0.7‰$ ($n = 24$). Though lithium is a dominant cation in all of our samples we also tested our analytical procedure in a sample with a more complicated matrix, and in which lithium is a trace element. We analyzed Bermuda seawater and obtained a δ^{7}Li value of 30.5‰ ($n = 3$), which is within error of the literature value for seawater [31‰, e.g. (Pogge Von Strandmann et al., 2013)].

2.5. Computational methods

Vibrational frequencies were calculated for a series of lithium complexes in order to provide a framework for the interpretation of measurements of isotopic fractionation between Li^{+}(aq) and lithiated gibbsite. The aqua ion Li^{+}(aq) was represented in threefold, fourfold, and sixfold coordination to solvation waters. The clay mineral environment is represented by a cluster cut from a layered double-hydroxide. Calculations were also conducted (see Supplemental Information) for ions with an association to Cl^{-} counter ions in order to assess how ion pairing may influence the results.

Isotope-fractionation factors were estimated from harmonic vibrational frequency calculations derived from density-functional theory electronic-structure calculations (DFT) on the representative molecules. Results are expressed in terms of reduced partition function ratios (RPFRs) for each lithium-coordination environment. Vibrational frequencies are calculated for the ^{7}Li- and ^{6}Li-centered molecules. The two lists of frequencies are used to calculate the RPFR using the methods in (Urey, 1947) (see the short code given in the Supporting Information). Calculations were carried out with the PQS 4.0 quantum chemistry code (Baker et al., 2012) using the 6-311++G(2d,2p) basis set and the B3PW91 exchange–correlation functional (Becke, 1993). Tight optimization/SCF thresholds and fine DFT integration grids were requested in all calculations. Aqua ions were modeled using methods laid out in Rustad et al. (2010). A complex consisting of the $[Li(H_2O)_n]^{+}$ ion surrounded by an explicit second solvation shell was fully optimized in the gas phase. The optimized complex was then embedded in COSMO continuum solvent (Klamt and Schüürmann, 1993) where the lithium ion and the first solvation shell were re-optimized while the second solvation shell was held fixed. The complexes are shown in Supplemental Fig. S3. The Hessian matrix of second derivatives $\partial^2 E/\partial\alpha_i\partial\beta_j$ was calculated numerically (displacement step size 0.02 bohr) for the mobile inner core (lithium ion plus first solvation shell). If a center of symmetry was present, it was used in construction of the Hessian matrix. Symmetry operations other than the symmetry center were not used in the construction of the Hessian matrix. Because

of the embedding, the number of degrees of freedom for the aqua ions is the full 3 N (30 for $[Li(H_2O)_3]^+$, 39 for $[Li(H_2O)_4]^+$ and 57 for $[Li(H_2O)_6]^+$). For reference, results are also given for the gas-phase $Li(H_2O)_3$ (C_1 symmetry), $Li(H_2O)_4$ (S_4 symmetry), and $Li(H_2O)_6$ (S_6 symmetry) ions. Because of the removal of translational degrees of freedom for the embedded ions, the Teller-Redlich product is 3/2 $\ln(m_{heavy}/m_{light}) = 0.230875709$. Rotational degrees of freedom for the gas-phase complexes, offered for reference, were not accounted for in the calculated fractionations.

The solid environment of the lithium was run using embedding methods that have been previously described (Rustad et al., 2008). A fragment of the gibbsite-like layer of the layered double-hydroxide structure was cut out around the central lithium ion (see Fig. 3d). Clipped bonds were terminated with bonds to partially-charged nuclei whose charges were chosen to conserve Pauling bond strength at the terminal oxide ion (clipped Al–O bonds were represented by +1/2 charges and clipped Li–O bonds were represented by +1/6 charges). These terminating nuclei were given hydrogen basis functions. Chloride ions were placed above and below the central lithium ion. Chloride ions on the vertical termination plane (light grey circles in Supplemental Fig. S3) were omitted, giving the cluster an overall +2 charge. Coordinates for all complexes are given in the Supporting Information.

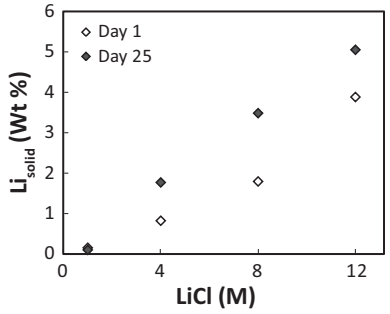

Fig. 1. A graph showing lithium loading as a function of the concentration of LiCl after 1 day and ~25 days.

3. RESULTS

3.1. Lithium intercalation

The amount of Li(I) intercalated into gibbsite varies with both the total electrolyte concentration and the identity of the counter ion. In the LiCl experiments, there is a clear positive relationship between Li(I) loading and total electrolyte concentration (LiCl; Fig. 1). In the 4 M, 8 M and 12 M LiCl experiments progressively more lithium was taken into gibbsite with time (See Table 2) while the amount of lithium incorporation into gibbsite from the 1 M LiCl experiment remained close to 0.1 wt% Li for the duration of the experiment. Results show that when Cl^- is the counter ion, far more lithium is taken up into gibbsite than with either NO_3^- or ClO_4^-. For example, using an electrolyte concentration of between 4 M and 5 M, after ~1 month the lithium concentration in gibbsite with Cl^-, ClO_4^- and NO_3^- as counter ions was >2 wt%, 0.1 wt% and 0.3 wt% respectively.

3.2. Isotopic analyses

The results of lithium-isotopic analyses are presented in Tables 2 and 3, and plotted in Figs. 2–5. Results show that at 25 °C both the total electrolyte concentration and identity of the counter ion influence the magnitude of isotopic fractionation associated with Li(I) intercalation into gibbsite. At higher temperatures (120 °C) there was no fractionation of lithium isotopes in either 1 M or 12 M LiCl solutions.

Starting with the LiCl experiments, we observe no isotopic fractionation during the reaction of gibbsite with 1 M LiCl but significant isotopic fractionations at higher concentrations (Figs. 2 and 3). Where isotopic fractionation occurs, ^6Li is always preferentially incorporated into the solid phase while the solution becomes correspondingly isotopically heavy. Due to the high concentrations of dissolved lithium salts in these experiments, changes in isotopic composition of the solution are negligible. After 25 days the magnitude of isotopic fractionation was relatively similar in the 4 M, 8 M, and 12 M experiments; with $\Delta^7Li_{solid\text{-}solution}$ values of −9.4‰, −8.4‰ and −6.4‰

Table 3
Li isotope and concentration data from experiments reacting end-solids from the 4 M and 8 M LiCl experiments with solutions of 1 M LiCl.

No. of hours	Molarity	T (°C)	δ^7Li (solution)	2σ	δ^7Li (solid)	2σ	$\Delta^7Li_{solid\text{-}solution}$	[Li_{solid}] wt%
4 M gibbsite reacted in 1 M LiCl								
Initial solid	1	25	4.5	0.3	−2.7	0.3	−7.2	3.45
1	1	25	4.9	0.4	−7.9	0.3	−12.7	2.73
5	1	25	5.0	0.3	−7.0	0.4	−11.9	2.41
24	1	25	4.8	0.1	6.6	0.2	−11.4	2.37
48	1	25	4.6	0.0	−6.8	0.4	−11.4	2.50
8 M gibbsite reacted in 1 M LiCl								
Initial solid	1	25	4.5	0.3	−5.8	0.4	−10.3	4.11
1	1	25	5.0	0.6	−12.7	0.1	−17.7	2.66
5	1	25	4.9	0.2	−12.2	0.2	−17.1	2.64
24	1	25	4.7	0.6	−11.6	0.4	−16.3	2.44
48	1	25	4.6	0.6	−11.6	0.2	−16.2	2.49

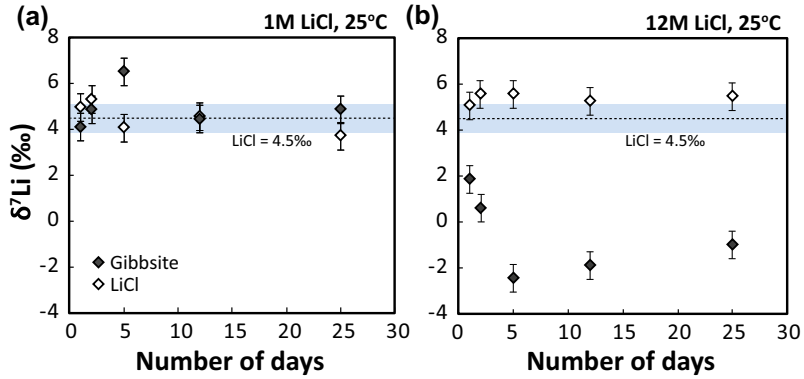

Fig. 2. Lithium-isotope data for solid and solution phases from 1 M and 12 M LiCl experiments. The starting LiCl solution has a δ^7Li value of +4.5‰, and the experiments were run for 25 days. All uncertainties are the 2σ external reproducibility (0.6‰), typical internal uncertainties are 0.1–0.3‰.

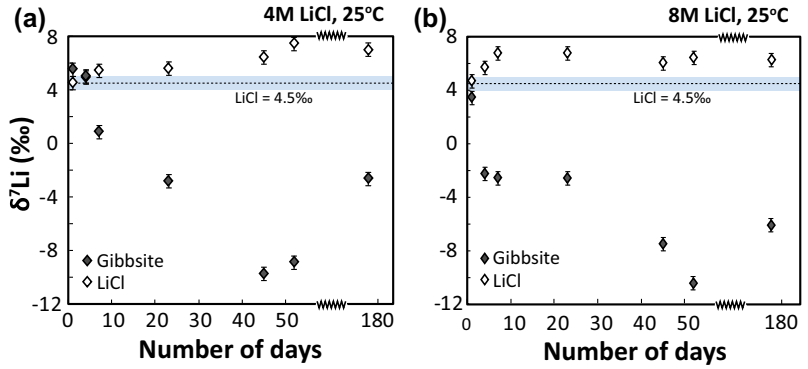

Fig. 3. Lithium-isotope data for solid and solution phases from 4 M and 8 M LiCl experiments. The starting LiCl solution has a δ^7Li value of +4.5‰, and the experiments were run for 177 days. All uncertainties are the 2σ external reproducibility (0.6‰), typical internal uncertainties are 0.1–0.3‰.

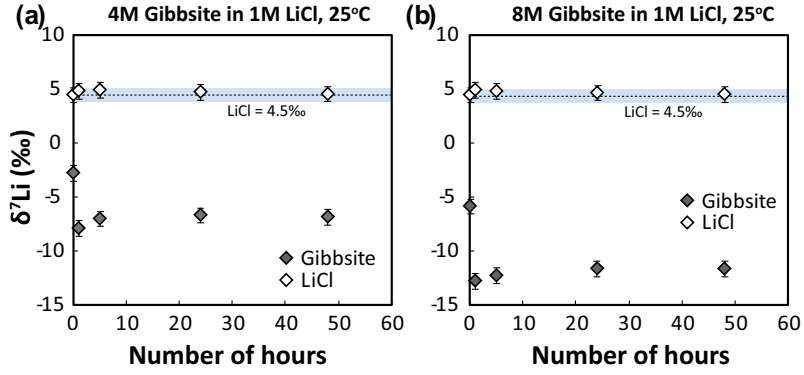

Fig. 4. Lithium-isotope data for solid and solution phases from experiments reacting end solids from the 4 M and 8 M LiCl experiments with 1 M LiCl. The LiCl solution has a δ^7Li value of +4.5‰, and the experiments were run for 48 h. All uncertainties are the 2σ external reproducibility (0.6‰), typical internal uncertainties are 0.1–0.3‰.

respectively. Sampling was continued for 177 days in the 4 M and 8 M experiments. In both we observe large changes in the amount of isotopic fractionation between solid and solution. After 52 days the $\Delta^7Li_{solid\text{-}solution}$ values decreased to −16.3‰ and −16.9‰ respectively before increasing to −2.7‰ and −9.9‰ respectively after 177 days (Fig. 3).

To examine this reversal of composition with time, we reacted gibbsite solid from the 4 M and 8 M LiCl experiments with a 1 M LiCl solution (Fig. 4). In both cases this reaction caused the solid to become relatively enriched in ^{6}Li. Final $\Delta^7Li_{solid\text{-}solution}$ values for the 4 M and 8 M solids were −11.4‰ and −16.2‰ respectively. The change in isotopic composition was accompanied by changes in solid

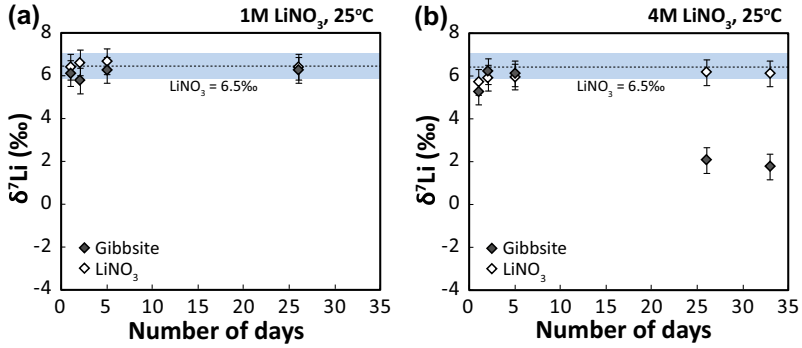

Fig. 5. Lithium-isotope data for solid and solution phases from 1 M and 4 M $LiNO_3$ experiments. The starting $LiNO_3$ solution has a δ^7Li value of +6.5‰, and the experiments were run for 25 days and 33 days. All uncertainties are the 2σ external reproducibility (0.6‰), typical internal uncertainties are 0.1–0.3‰.

Table 4
Reduced partition function ratios (calculated at 298.15 K) for complexes investigated in this paper.

	Gas	2nd Shell + COSMO
$[Li(H_2O)_3]^+$	1.075	1.071
$[Li(H_2O)_4]^+$	1.074	1.068
$[Li(H_2O)_6]^+$	1.045	1.033
LDH	1.065	

Table 5
Calculated fractionation factors ($1000\ln(\alpha_{aq}/\alpha_{LDH})$).

	$[Li(H_2O)_3]^+$	$[Li(H_2O)_4]^+$	$[Li(H_2O)_6]^+$
LDH	+5.6	+2.8	−30.5

composition. When the gibbsite solid from the 4 M and 8 M LiCl experiments was reacted with a new solution of 1 M LiCl, the lithium concentration of the gibbsite decreased; the lithium concentration in this gibbsite from the 4 M experiment decreased by ~1 wt% and the gibbsite from the 8 M experiment decreased by ~1.5 wt% (see Table 3).

The effect of total concentration on isotope fractionation was also observed by comparing the reaction of gibbsite with 1 M and 4 M $LiNO_3$ solutions. Similar to the results of the LiCl experiment there was no isotopic fractionation of lithium isotopes in the 1 M $LiNO_3$ experiment. In the 4 M $LiNO_3$ experiment the $\Delta^7Li_{solid\text{-}solution}$ was −4.3‰ after 33 days (Fig. 5).

The effect of the counter ion on the isotopic fractionation of lithium is best illustrated through comparison of $\Delta^7Li_{solid\text{-}solution}$ values in experiments of similar total concentration and ionic strength. If experiments with 5 M LiCl, 5 M $LiClO_4$ and 4 M $LiNO_3$ are compared we observe maximum $\Delta^7Li_{solid\text{-}solution}$ values of −16.3‰, −0.1‰ and −4.3‰ respectively. Thus the amount of isotopic fractionation increases in the counter ion order $ClO_4^- < NO_3^- < Cl^-$.

3.3. Calculations of isotope fractionation

The calculations indicate that only a small isotopic fractionation could arise from changes in ion solvation. The results of the calculations are given in Tables 4 and 5. For the aqua ions, findings are similar to previous work on the Li^+(aq) (Yamaji et al., 2001; Kowalski and Jahn, 2011), with a large fractionation predicted between $[Li(H_2O)_4]^+$ and $[Li(H_2O)_6]^+$, and a small fractionation predicted between $[Li(H_2O)_3]^+$ and $[Li(H_2O)_4]^+$. The fractionation predicted between the aqua ions and the layered double-hydroxide environment is similar to that calculated between aqua ions in lithiated mica in Kowalski and Jahn (2011).

3.4. XRD analyses

The experiments sampled for XRD were: 4 M and 8 M solids and experiments where 4 M and 8 M solids were redispersed in solutions of 1 M LiCl. All experiments successfully intercalated lithium ions into the gibbsite mineral lattice, as expected from the previous work (XRD patterns in Supplemental Fig. S5).

3.5. NMR spectroscopy

Progressive formation of the $[LiAl_2(OH)_6]Cl.nH_2O$ is evident in both the ^{27}Al- and ^{7}Li-MAS-NMR spectra and this reaction correlates well with the isotopic fractionation. The ^{7}Li-MAS-NMR data indicate at least two coordinatively distinct lithium sites in the reacted gibbsite lattice. A relatively narrow signal with two singularities centered at −0.2 ppm indicates the presence of a well-defined octahedral site in the layered double-hydroxide mineral, while the broad feature at about 0 ppm is consistent with amorphous lithium-containing phases with disordered local structure e.g. surface or various local structures. We observe, however, little evidence for formation of the $[LiAl_2(OH)_6]Cl.nH_2O$ phase from gibbsite in the 1 M solutions at room temperature (Fig. 6a and b). Similarly, the ^{27}Al-MAS-NMR spectra of the samples after days of reaction are unmodified and indicate two distinct ^{27}Al sites with second-order quadrupolar patterns, as is expected from well-crystallized gibbsite (Ashbrook et al., 2000) (Fig. 6a).

Fig. 6b shows the ^{27}Al-NMR spectra of the samples in 4 M, 8 M and 12 M and one can see that a single peak is evident in the samples. This peak corresponds to the

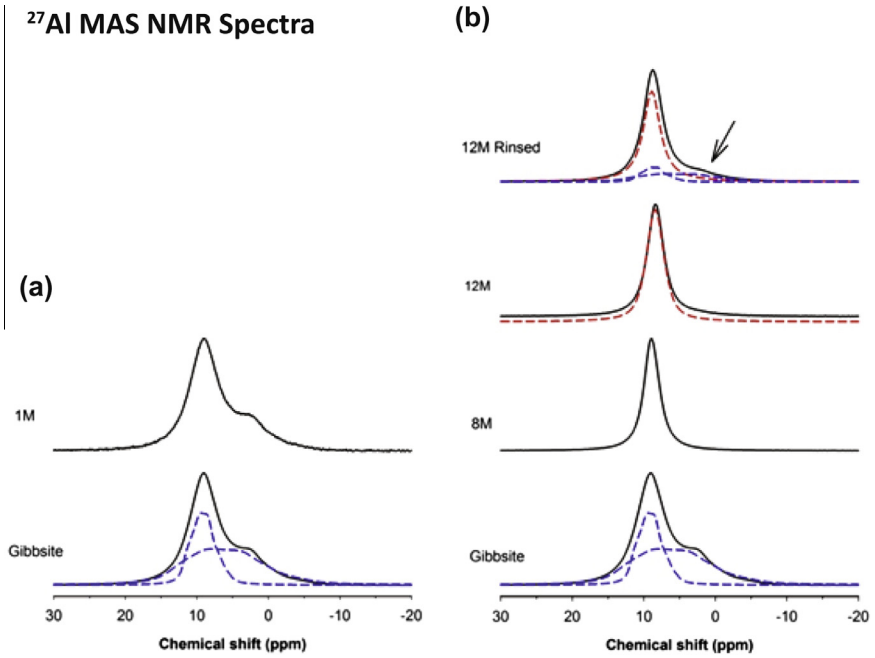

Fig. 6. (a) ^{27}Al MAS NMR spectra of gibbsite and a sample prepared with 1 M LiCl solution. The reaction product has the feature of gibbsite, which is consistent with the XRD results for these samples. (b) ^{27}Al MAS NMR spectra of samples prepared with higher concentration of LiCl solutions. The ^{27}Al NMR spectra of the samples reacted in 8 M and 12 M solutions have one signal, which is characteristic of the $[LiAl_2(OH)_6]Cl.nH_2O$ layered double-hydroxide (Hou and Kirkpatrick, 2001)). Upon rinsing, however, the ^{27}Al spectra show evidence of the reaction reversing, and forming gibbsite from the $[LiAl_2(OH)_6]Cl.nH_2O$ layered double-hydroxide solid. The sample at top was agitated in an ultrasonic bath for two five-minute rinses with distilled water. With this gentle treatment, the peak assignable to the $[LiAl_2(OH)_6]Cl.nH_2O$ solid broadens and the two-site spectra that is characteristic of gibbsite becomes evident.

$[LiAl_2(OH)_6]Cl.nH_2O$ phase and exhibits a single narrow signal at about 8.5 ppm, corresponding to $[LiAl_2(OH)_6]Cl.nH_2O$ (Hou and Kirkpatrick, 2001)). The ^{7}Li MAS-NMR spectra also indicate a typical second-order quadrupolar pattern, as expected for ^{7}Li in octahedral sites with nearly uni-axial symmetry. Using the deconvolution software DMFIT (Massiot et al., 2002), we calculated a quadruple coupling constant of 0.456 MHz, $= 0.104$, isotropic chemical shift $= -0.4$ ppm for this site.

For most, but not all samples, however, the ^{7}Li-NMR spectra also indicate the presence of two sites in varying concentrations. A broad feature is evident in samples early in a reaction set, or if the samples were wetted after extraction, such as in rinsing experiments. This broad feature is consistent with ^{7}Li in an amorphous setting and is centered near 0 ppm (Fig. 7), underlying the relatively well defined feature that we assign to ^{7}Li in the layered double-hydroxide phase. However, no second lithium-containing phase was evident in the X-ray diffraction patterns of the lithiated solids (Supplemental Information), even in samples where this broad feature was clearly evident in the ^{7}Li-NMR spectra. This second broad peak could not be crystalline LiCl formed during drying as it was not detected in X-ray diffraction and because the ^{7}Li NMR peak is much too broad to be assignable to such a well-crystallized material as LiCl.

We also noticed that the ^{7}Li NMR spectra of layered double-hydroxide samples made with 12 M LiCl solutions evolved over time, consistent with distortions of the $Li(OH)_6$ octahedral structures and strong displacements of the lithium ions. One can also see in both the ^{27}Al- and ^{7}Li-NMR spectra that the lithiation is partly (and rapidly) reversible upon rinsing, as a shoulder immediately becomes evident upfield from the main and broad ^{27}Al assigned to the $[LiAl_2(OH)_6]Cl.nH_2O$ solid and, upon rinsing, the peak broadens. The rapid reversing of the intercalation and return of the structure to a gibbsite-like phase is even more evident in the ^{7}Li-MAS-NMR data, where rinsing with distilled water causes most of the ^{7}Li-NMR signal to disappear and the layered double-hydroxide solid to collapse. Thus the NMR data indicate two reservoirs for lithium, only one of which has a well-defined structural setting.

4. DISCUSSION

Experiments show that temperature, electrolyte concentration, and counter ion identity all influence the isotopic fractionation. In the following discussion we consider each of these three parameters turn.

4.1. Temperature

The effect of temperature is unsurprising and clear. Our data show no isotopic fractionation of lithium at 120 °C in 12 M LiCl, while the same experiment had a $\Delta^7Li_{solid\text{-}solution}$ value of $-6.5‰$ at 25 °C (see Table 2). This result is fully consistent with previous work by Vigier et al. (2008) and

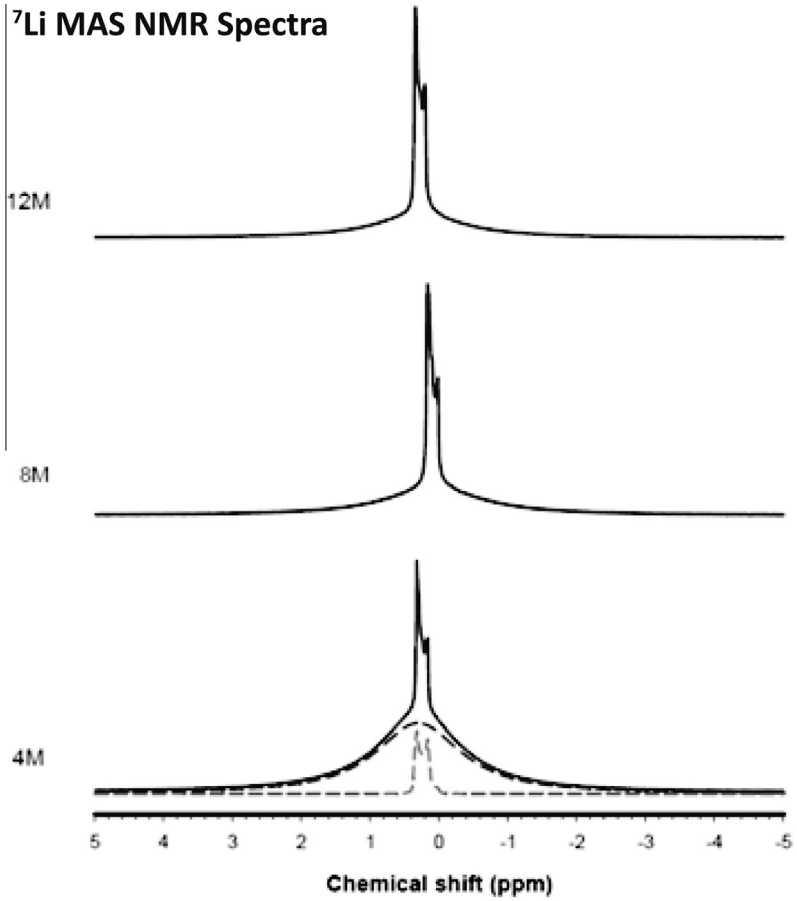

Fig. 7. ^{7}Li MAS-NMR spectra of samples prepared with LiCl solutions. All ^{7}Li spectra exhibit two components. The first is a broad signal that has a mixed Gaussian/Lorentzian line shape ($G/L = 0.1$) centered near 0.31 ppm with a width of 293 Hz. This signal is identified in the lowermost figure as the bolder dashed line. Another signal is relatively narrow and has a pattern consistent with a second-order quadrupolar environment. This signal is shown as the grey dashed line in the lowermost spectrum. In general, this narrow feature becomes more evident with progressive double-hydroxide solid formation and is assignable to Li(I) in the well-defined octahedral site in the layered double-hydroxide mineral. The fitted pattern is centered over 0.41 ppm, has a quadrupolar coupling constant of 0.5 MHz, line-broadening of 3.5 Hz and an asymmetry parameter, $\eta = 0.2$.

Nishizawa et al. (1984a), and is expected from the fundamental thermodynamics of equilibrium-isotopic fractionation (Urey, 1947), i.e. that we observe more stable-isotope fractionation at lower temperatures. Although we do not observe the same temperature dependence in the 1 M LiCl experiment the intercalation rate of Li into gibbsite is much slower in lower molarity solutions (e.g. Fogg and O'Hare, 1999). Thus the Li isotope data from the two 12 M experiments can be compared purely in terms of the effect of temperature, while in the 1 M experiments we must also consider the extent of reaction. The relationship between electrolyte molarity and reaction extent is discussed in more detail in Section 4.2.

It is important to reiterate that the temperature dependence of lithium-isotope fractionation continues below 90–120 °C. Vigier et al. (2008) found no change in the isotopic fractionation factor below 90 °C during uptake of lithium into smectite, however they hypothesize that this was a misleading result caused by the reaction not reaching equilibrium at lower temperatures. The data of Nishizawa et al. (1984a) shows that temperature effects can occur during uptake of lithium into cryptand resin at low temperatures over a very limited range from 0 to 40 °C. Our data shows that there is a considerable difference in $\Delta^{7}Li_{solid\text{-}solution}$ between experiments performed at 25 and 120 °C. Even so, it is difficult to make robust conclusions about the relationship between the fractionation factor and temperature from just two data points; clearly more experiments would be necessary to fully quantify this relationship.

4.2. Electrolyte concentration

Our data appear to be broadly consistent with that of Nishizawa et al. (1988), i.e. that greater isotopic fractionation is observed at higher electrolyte concentrations (Figs. 2–5). There are, however, two effects hidden in this phenomenon because the activity of water scales with the total concentration of lithium electrolyte. A reduced activity of water is consistent with the hypothesis that the

lithium coordination number would be lower at higher electrolyte concentrations and would affect isotopic fractionation during incorporation of lithium into the six-membered ring of gibbsite; one expects the fractionation to increase. However, the relationship between $\Delta^7Li_{solid\text{-}solution}$ and electrolyte concentration is actually not straightforward; $\Delta^7Li_{solid\text{-}solution}$ does not linearly increase with lithium molarity. For example, if we just consider the LiCl experiments then the $\Delta^7Li_{solid\text{-}solution}$ values obtained in the 12 M LiCl experiment are lower than values obtained using 4 M and 8 M after ~25 days (see Section 3.3. and Table 2).

The DFT calculations are consistent with previous work and show that changing lithium speciation from $Li(H_2O)_4]^+$ to $[Li(H_2O)_3]^+$ would have a negligible effect on isotopic fractionation. Although it is reasonable to expect that variations in the activity of water reduce the solvation number of Li^+(aq) (between $[Li(H_2O)_4]^+$ and $[Li(H_2O)_3]^+$) these changes would not result in much difference in the fractionation against a constant reference compound like the lithiated gibbsite. In other words both our calculations, as well as those of Kowalski and Jahn, 2011, suggest that the large range in isotopic fractionations observed in our experimental study cannot simply be caused by different electrolyte concentrations changing the coordination number of Li^+(aq) in solution. In addition, estimates of the effects of ion pairing (e.g., $[LiCl]^0$) indicate small effects on the reduced partition function ratio (RPFR) of Li^+(aq) and indicate that progressive ion pair formation is unlikely to be responsible for driving large fractionations (see Supplemental Information). Our calculations, as well as those of Kowalski and Jahn, show that $[Li(H_2O)_6]^+$ has a dramatically lower RPFR than both $[Li(H_2O)_4]^+$ and $[Li(H_2O)_3]^+$, but this cannot account for the observed fractionation because the six-coordinated lithium aqua ion would be predicted to be isotopically lighter than lithium in the LDH, which our experiments show is not the case. We conclude that there must be another mechanism that relates higher electrolyte concentrations with larger $\Delta^7Li_{solid\text{-}solution}$ values.

It is helpful to consider that, unlike the macrocyclic compounds studied by Nishizawa and coworkers, gibbsite has a layered structure and the amount of lithium taken into the gibbsite (the lithium loading) varies within and between different experiments. As shown by Fogg and O'Hare (1999) and Williams and O'Hare (2006) the mechanism of lithium intercalation into gibbsite is such that rates are limited by the expansion of the interlayer. This means that, upon loading, the Li(I) and counter ion first move into the expanded interlayer before the Li(I) can fill the octahedral vacancies; that is, the diffusion probably occurs by a coupled ion-pair movement of the cation and anion together. We don't know the stoichiometry or structure of the diffusing species, but the need to maintain a charge balance in the clay suggests that the movement of the cation and anion must be correlated. Furthermore, the fact that the most rapid rates correspond to the smallest monatomic counter ion, Cl^-, suggest that an inner-sphere complex like $LiCl^0$ may be the most rapidly diffusing moiety as the solid structure reorganizes.

As shown in Fig. 8, there is a rough trend showing that increased lithium loading corresponds to more negative $\Delta^7Li_{solid\text{-}solution}$ values. Because the unreacted gibbsite contains negligible lithium, this relationship cannot be caused by two-component mixing. Rather, the isotopic fractionation must arise kinetically from the intercalation process itself, or as an equilibrium effect by chemical bonding of lithium to the octahedral vacancies in gibbsite. SEM analyses of the gibbsite reacted with 1 M, 4 M and 12 M LiCl clearly show evidence for interlayer expansion (Fig. 9), with more prominent expansion visible at the higher molarities (4 M and 12 M), coincident with increased lithium loading (Fig. 1). Thus, it is likely that the $\Delta^7Li_{solid\text{-}solution}$ value is related to the amount of lithium that is taken up purely through diffusion into the expanded interlayer. Some of this lithium will be chemically bound to octahedral vacancies with the counter ion placement causing expansion of the structure. What is unclear is whether all of the intercalated lithium will end up bound to the octahedral sheet or whether some will remain in the interlayer and at edges. This distinction will have consequences for the final δ^7Li value of the solid and is discussed in more detail in Section 4.4.

It is interesting to note that where loading of lithium into gibbsite is small (0.1–1 wt%) there is negligible fractionation of lithium isotopes (Figs. 2 and 5). This result is in direct contrast to observations of lithium isotope behavior in natural systems and other experimental studies involving weathering reactions (e.g. Chan et al., 1992; Pistiner and Henderson, 2003; Wimpenny et al., 2010a,b) where significant isotopic fractionation of lithium is observed. These results can be explained if we consider the kinetics of lithium intercalation into gibbsite (Fogg and O'Hare, 1999; Williams and O'Hare, 2006). We hypothesise that at lower total dissolved lithium concentrations the intercalation of lithium is either much slower, or that the expansion of the interlayer cannot occur, at least

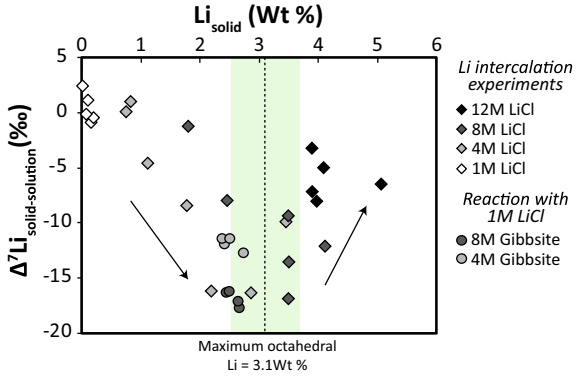

Fig. 8. A graph showing the fractionation of lithium isotopes between solid and solution during uptake of lithium into gibbsite ($\Delta^7Li_{solid\text{-}solution}$) as a function of lithium loading for all experiments performed using LiCl solutions. There is a rough first-order correlation between Li loading and $\Delta^7Li_{solid\text{-}solution}$. However in more detail it appears that the maximum isotopic fractionation coincides with lithium loading of between 2.5 and 3.5 wt%. Above this concentration the $\Delta^7Li_{solid\text{-}solution}$ value decreases again.

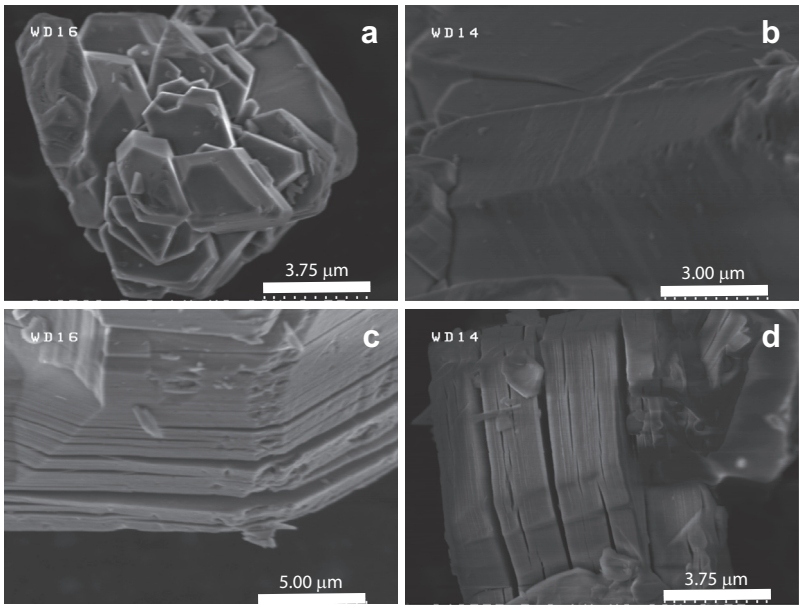

Fig. 9. Scanning electron micrographs of (a) unreacted gibbsite, (b) gibbsite reacted with a 1 M LiCl solution, (c) gibbsite reacted with a 4 M LiCl solution, and (d) gibbsite reacted with a 12 M LiCl solution.

over the timescales of our experiments. Perhaps at lower ionic strength it takes much longer for interlayer expansion and incorporation to occur, and further diffusion of lithium counter-ion ion pairs within the interlayer is also very slow. Certainly the SEM images of gibbsite reacted with 1 M LiCl show far less prominent layer expansion than at 4 M or 12 M (Fig. 9). These data imply that over a relatively short timescale (on the order of weeks) and without interlayer expansion, the uptake of lithium occurs with no isotopic preference, i.e. the phase change facilitates lithium intercalation into gibbsite and induces the isotopic fractionation. One expects such chemistry if a threshold concentration of lithium was needed to induce the phase change.

Another interesting observation is that little or no isotopic fractionation was observed during the first 4 days of reaction of gibbsite with 4 M LiCl despite solid-phase lithium concentrations of ~0.8 wt%. In this case the lithium loading was up to 8 times greater than lithium loading in the 1 M LiCl experiments, implying that some interlayer expansion and intercalation of lithium had occurred. Despite this intercalation, there was no accompanying isotopic fractionation of lithium. This suggests that the intercalation of lithium into the gibbsite interlayer itself does not cause isotopic fractionation. Instead, the fractionation must be caused by either diffusion of lithium within the interlayer, or by the final incorporation of lithium into the octahedral vacancies. Based on our experimental data we cannot exclude either hypothesis, and in fact both processes (diffusion and site occupancy) may play a role.

4.3. Counter-ion identity

The lithium-isotopic fractionation associated with lithiation of gibbsite increases in the counter-ion order $ClO_4^- < NO_3^- < Cl^-$. Similar to our observations in Section 4.2. This difference appears to be related to lithium loading. Fogg and O'Hare (1999) show that the nature of the anion affects the intercalation rate of lithium into gibbsite, and that the rate of intercalation is roughly correlated with radius of the anion, as one expects from a process of diffusion. The ionic radii of the counter ions in the current study are 0.241 nm, 0.177 nm, and 0.180 nm for ClO_4^-, NO_3^- and Cl^- respectively (Marcus, 1988). While perchlorate has the largest radius, which might explain why the lithium loading was so low, the nitrate and chloride ions are almost identical in size but lithium loading is far greater with Cl^- as the counter ion.

Williams and O'Hare (2006) investigated several other counter-ions and came to the conclusion that neither hydration enthalpy, charge distribution, activation energy nor ionic radius can fully explain why the anion identity affects the intercalation kinetics. The charge in the Cl^- is, of course, more localized than in the NO_3^-, which may be important if the diffusing moiety were an inner-sphere ion pair, like $LiCl^0$, as we mentioned above. These differences, even if poorly explained, are also manifested in the isotope fractionation.

Nishizawa et al. (1984b) showed the counter ion also affected the fractionation factor for lithium uptake into benzo-15-crown-5. In this case the least amount of fractionation was associated with Cl^- and the most with I^-; i.e., most fractionation was associated with the anion with the largest ionic radius. While this is the opposite trend to that observed in the current study, Nishizawa and coworkers used methanol as a solvent. Moreover, fundamental differences in structure between benzo-15-crown-5 and gibbsite mean that factors influencing intercalation rate of lithium into gibbsite, including counter-ion identity, would not necessarily affect macrocyclic compounds in the same way. It nevertheless is interesting that counterions remain important even in situations where there is no large-scale structural transformation.

4.4. Quantifying isotope fractionation

The results show that $\Delta^7Li_{solid\text{-}solution}$ is influenced by temperature, electrolyte concentration, and counter ion. However, the relationships between these factors and $\Delta^7Li_{solid\text{-}solution}$ are not straightforward as we must take into account associated changes in the gibbsite structure that in turn influence lithium loading. Ultimately, this makes interpreting $\Delta^7Li_{solid\text{-}solution}$ values equivocal.

To address this question, it is first useful to consider the lithium mass balance, i.e. to what extent have the octahedral vacancies been filled in each experiment? In the case of experiments with the NO_3^- and ClO_4^- salts, lithium loading was small so the maximum percentage of octahedral sites filled is also small, usually <10%. However, much more lithium loading occurred in the Cl^- experiments. In this case the idealized formula of the solid is $[LiAl_2(OH)_6]Cl.1.5H_2O$ and the maximum lithium concentration should be 3.1 wt% [e.g. (Tarasov et al., 2004)]. As shown in Fig. 8 the gibbsite samples had lithium concentrations that ranged from 0.1 to 5.1 wt%, with several samples from the 4 M, 8 M and 12 M LiCl experiments having lithium concentrations greater than 3.1 wt%.

In other words, some experiments loaded lithium into the gibbsite in amounts that exceed the concentration of six-membered oxo rings that are essential for making the layered double-hydroxide solid. If we look in more detail Fig. 8 actually shows an intriguing relationship between lithium loading and $\Delta^7Li_{solid\text{-}solution}$. As lithium loading increases from 0 to ~3.1 wt% the $\Delta^7Li_{solid\text{-}solution}$ values become highly negative, however as lithium loading continues to increase from ~3.1 to 5 wt% the $\Delta^7Li_{solid\text{-}solution}$ values become less negative again. These observations can be explained if lithium occupies at least two sites, or perhaps better described as two reservoirs, and that these reservoirs contain lithium with distinctly different δ^7Li values. If the isotopic composition of lithium in these two reservoirs differ, then the δ^7Li value of the bulk solid will be controlled, not only by the isotopic composition of lithium in these sites, but also by the relative proportion of octahedral lithium in the two reservoirs, which varies with loading and reaction history.

Solid-state ^7Li and ^{27}Al NMR spectra (see Section 3.5) show clear evidence for two reservoirs and one reservoir is well understood – the octahedral sites that form the layered double-hydroxide solid where the lithium is held by inner-sphere coordination to structural oxygens. We assign this reservoir to the narrow, second-order quadrupolar signal in ^7Li-NMR spectra. The site becomes clear when ^{27}Al-NMR spectra indicate that the gibbsite has converted to the layered double-hydroxide (Fig 7). The second reservoir corresponds to a broad feature in the ^7Li-NMR spectra that indicates a poorly organized structure, such as interlayer Li(I) or adsorbed lithium. The lithium in this reservoir is sufficiently disordered to give a wide range of chemical shifts.

We infer that isotopic fractionation into this second reservoir of lithium sites is near zero, as would be found if the adsorbates or interlayer ions were structurally similar to lithium solutes. While the δ^7Li value of lithium in the second reservoir was not directly measured, the assertion that it is taken up from solution with little or no isotopic fractionation can explain several of our experimental observations and is consistent with uptake of magnesium into the interlayer in smectite (Wimpenny et al., 2014). For example the maximum $\Delta^7Li_{solid\text{-}solution}$ values in the 12 M LiCl experiment are much smaller than in the 4 M and 8 M experiments (−8‰ compared to −16‰) despite the gibbsite experiencing more prominent interlayer expansion (Fig. 9d) and becoming more rapidly loaded with lithium (3.9 wt% after just 1 day). These observations can be explained if the octahedral vacancies were filled rapidly due to more rapid intercalation of lithium in higher molarity solutions, as demonstrated in Fogg and O'Hare, 1999. Once the available octahedral sites were filled any further loading of lithium could only occur as solvated adsorbates or solvated interlayer ions. If uptake of this solvated lithium does so with little or no isotopic fractionation, then it would drive the bulk gibbsite to isotopically heavier values. In the 12 M LiCl experiment we hypothesize that this process occurred so quickly that interlayer expansion and saturation of the octahedral sheet occurred from the first sample (24 h).

This two-reservoir hypothesis explains the trend in Fig. 8; in solids with more than 2.5–3.5 wt% Li it is likely that most of the available octahedral sites have already been filled. In this case any additional lithium is driving the solid to increasingly heavy δ^7Li values and hence $\Delta^7Li_{solid\text{-}solution}$ values become less negative. Further evidence for the two-reservoir hypothesis is provided from reacting the final solids from the 4 M and 8 M LiCl experiments with a solution of 1 M LiCl (Fig. 4). In both cases the gibbsite lost lithium and the δ^7Li values of the solid decreased by between 4‰ and 6‰. We strongly suspect that the loss of lithium probably occurred as a result of contraction of the initially expanded interlayer. If this lithium has a similar δ^7Li value to lithium in the fluid phase (i.e.+4.5‰ to +7‰) then its loss must drive the solid phase to isotopically lighter δ^7Li values, consistent with observation (Fig. 4). This explanation is also supported by simple mass-balance calculations (see Table 6). The similarity between the δ^7Li value of the measured gibbsite and our calculated values suggest that our hypothesis is robust. The dependence of $\Delta^7Li_{solid\text{-}solution}$ on lithium loading, and the presence of two lithium sites in gibbsite is summarized in a simple schematic diagram (Fig. 10).

Our data suggest that the maximum $\Delta^7Li_{solid\text{-}solution}$ value is approximately −16‰, but this value is likely to underestimate the true fractionation factor (α) associated with binding of lithium to octahedral vacancies in inner-sphere coordination. The value is complicated by parallel uptake of adsorbates and solvated interlayer ions so that one must calculate the relative proportion of lithium in both reservoirs in order to calculate a meaningful fractionation factor. As discussed, the idealized lithiated gibbsite contains a maximum of 3.1 wt% Li if the metal is only bound to the six-membered μ_2-oxo rings. However, there is strong evidence from the $^{6,7}L$-NMR data that a solid with 3.1 wt% Li has only a portion of this lithium in the octahedral sheet. Also, because the intercalation of lithium into gibbsite is controlled by expansion of the interlayer any sensitivity of α to either electrolyte concentration

Table 6
Upon the reaction of end-solids from the 4 M and 8 M experiments with 1 M LiCl the gibbsite loses Li and its bulk δ^7Li value becomes fractionated. This mass balance calculation shows that the shift in δ^7Li can be satisfactorily explained by straightforward loss of interlayer Li that was initially taken up from solution with no isotopic fractionation (see comparison between calculated and measured initial gibbsite δ^7Li values in bold).

	Gibbsite from 4 M LiCl exp.	Gibbsite from 8 M LiCl exp.
Initial gibbsite [Li] wt%	3.45	4.11
Final gibbsite [Li] wt%	2.5	2.49
Proportion of Li lost from the gibbsite	0.28	0.39
Assumed proportion of octahedral Li	0.72	0.61
Final gibbsite δ^7Li (assumed octahedral δ^7Li)	−6.8	−11.6
Fluid phase δ^7Li (assumed interlayer δ^7Li)	7.2	6.3
Calculated initial gibbsite δ^7Li	**−2.9**	**−6.6**
Measured initial gibbsite δ^7Li	**−2.7**	**−5.8**

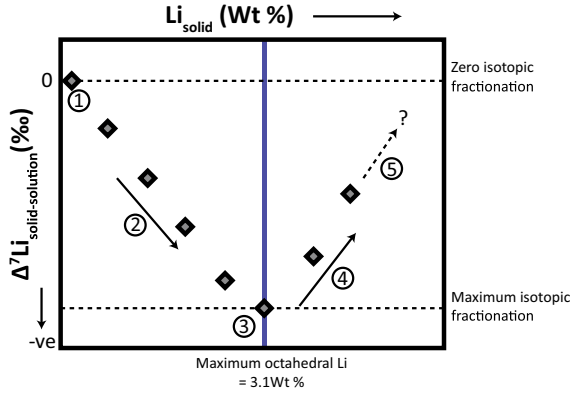

Fig. 10. A simple schematic illustrating how the lithium-isotopic fractionation ($\Delta^7Li_{solid\text{-}solution}$) associated with uptake of lithium into gibbsite reflects lithium loading. Initially the gibbsite contains little or no lithium and so $\Delta^7Li_{solid\text{-}solution}$ must be close to zero (1). As the gibbsite interlayer swells, lithium diffuses into the interlayer, with little or no isotopic preference, and from here can fill vacant octahedral sites with a preference for ^{6}Li. As a consequence the $\Delta^7Li_{solid\text{-}solution}$ value becomes more negative (2). This fractionation reaches a maximum when all of the available octahedral spaces are filled and the phase change is complete (3). Obviously diffusion-controlled fractionation may also contribute. More expansion and loading occurs with continued lithium uptake into the interlayer but no more octahedral incorporation. Because its δ^7Li value reflects lithium in solution the interlayer Li is relatively isotopically heavy and so the $\Delta^7Li_{solid\text{-}solution}$ value must decrease (4). The final $\Delta^7Li_{solid\text{-}solution}$ value reflects the mass balance between lithium in the octahedral site and lithium in the interlayer. However because some lithium remains bound in the octahedral site the final $\Delta^7Li_{solid\text{-}solution}$ must be <0 (5).

or counter ion identity is superseded by fluid chemistry that either inhibits or promotes expansion of the interlayer.

5. IMPLICATIONS

The use of lithium isotopes to trace past changes in weathering and climate relies on accurate knowledge of how its isotopes behave during mineral reactions. Our results highlight that even in seemingly simple layered clay minerals such as gibbsite the behavior of lithium is not straightforward, so that the difference in δ^7Li between the bulk solid and accompanying fluid phase cannot be characterized by a single fractionation factor. While previous experimental studies (e.g. Pistiner and Henderson, 2003, Vigier et al., 2008) provide valuable information about the sense and magnitude of Li isotope fractionation during mineral–fluid interaction it is clear that detailed knowledge of the proportion and isotopic fractionation associated with uptake into different host sites (e.g. octahedral sheet, interlayer etc.) are needed to accurately quantify fractionation factors.

We show that for lithium intercalation into gibbsite the factors that facilitate uptake of cations into the clay structure (such as electrolyte concentration and counter-ion identity) also control the rate at which isotopic fractionation occurs, but it is unclear from our data whether these factors influence the fractionation factor associated with octahedral binding of lithium. Data showing lithium isotope fractionation with lithium loading (Fig. 8) suggests that the fractionation factor does not change significantly with electrolyte concentration but further research will be necessary to investigate these reactions in more detail. The implications of these data for understanding stable isotope fractionation during weathering are not straightforward due to the complexity of natural systems. However, the behavior of Li isotopes during intercalation into gibbsite is consistent with that of magnesium isotopes during uptake into clay-rich soils (e.g. Opfergelt et al., 2012, 2014) and exchange into clay minerals such as smectite and illite (Wimpenny et al., 2014). The uptake of Li into exchangeable sites with no isotopic preference will result in the δ^7Li value of bulk clay minerals being driven to increasingly positive values, assuming that river waters and seawater contain isotopically heavier Li than silicate minerals (e.g. Huh et al. 1998, Kisakurek et al., 2005, Millot et al. 2010). To a first order, our results suggest that bulk analyses of the δ^7Li value of clay minerals and clay rich sediments will result in underestimation of any isotopic fractionation that occurs during weathering. Ultimately however, the δ^7Li value of a bulk sediment sample will depend on many factors; these include the clay content, the relative abundance and δ^7Li value of Li present in exchangeable and chemically bound sites, and the δ^7Li value of the fluid phase. The findings from this study will be important in understanding and quantifying the isotopic fractionation associated with elemental uptake into

secondary minerals and clay rich sediments, particularly sediments rich in layered minerals such as smectite and illite that have a large cation exchange capacity. Further work will be necessary to characterize how different physico-chemical parameters influence the fractionation factor of Li during octahedral binding in clay minerals. In addition to temperature, electrolyte molarity and counter ion identity, factors not considered here such as solution pH and clay mineral structure may also be important.

6. CONCLUSIONS

Lithium isotopes become fractionated during conversion of gibbsite into the layered-double-hydroxide mineral that contains lithium in well-defined six-membered oxo rings. Temperature, electrolyte concentration and the counter ion all influence the extent of reaction and the $\Delta^7Li_{solid\text{-}solution}$ value. The relationship between isotopic fractionation and reaction progress, however, is not simple and NMR spectra identify at least two reservoirs for lithium that vary in importance with the amount of lithium loading and that store lithium with very different isotopic compositions. One reservoir is clearly the six-membered oxo ring that takes up lithium in inner-sphere coordination. This partitioning has a strong preference for ^6Li in the solid phase and leaving the residual fluid isotopically heavy. The second reservoir is a disordered ensemble of sites with a range of ^7Li-NMR chemical shifts. There also appears be little or no fractionation relative to the solutes, suggesting that these sites are solvated adsorbates or interlayer ions.

Therefore an experiment commonly exhibits two stages of $\Delta^7Li_{solid\text{-}solution}$ fractionation, depending upon the lithium loading. In stage one, the expansion of the gibbsite structure causes lithium to diffuse into the interlayer and fill octahedral vacancies, making the $\Delta^7Li_{solid\text{-}solution}$ value increasingly negative. The diffusion step may be important to the isotopic fractionation; we cannot constrain this question in our study. With increased loading, a second stage becomes evident. In stage two, octahedral vacancies are all filled and uptake of lithium from solution involves relatively weak bonding at surface and into the interlayer. Hence continued loading causes the solid to become increasingly isotopically heavy, reducing the $\Delta^7Li_{solid\text{-}solution}$ value.

ACKNOWLEDGEMENTS

This work was supported by NASA grant NNX07AV56G to WHC, Q-ZY, and JRR. The authors thank Prof. Alexandra Navrotsky, Drs. P. Saradhi Maram and Sergey Ushakov for help with the powder X-ray diffractometry. The authors would also like to thank Dr. Shailise Ross for help with the acquisition of the SEM photomicrographs. This manuscript benefitted from the insightful comments of Weiqiang Li and three anonymous reviewers, and the editorial handling of Fang-Zhen Teng.

APPENDIX A. SUPPLEMENTARY DATA

Supplementary data associated with this article can be found, in the online version, at http://dx.doi.org/10.1016/j.gca.2015.07.011.

REFERENCES

Ashbrook S. E., McManus J., MacKenzie K. J. D. and Wimperis S. (2000) Multiple-quantum and cross-polarized ^{27}Al MAS NMR of mechanically treated mixtures of kaolinite and gibbsite. *J. Phys. Chem. B* **104**, 6408–6416.

Badger R. M. (1934) A relation between internuclear distances and bond force constants. *J. Chem. Phys.* **2**(3), 128–131.

Baker J., Janowski T., Wolinski K. and Pulay P. (2012) Recent developments in the PQS program. *Wiley Interdis. Rev.: Comput. Mol. Sci.* **2**(1), 63–72.

Ban Y., Nomura M. and Fujii Y. (2002) Chromatographic separation of lithium isotopes with silica based monobenzo-15-crown-5 resin. *J. Nucl. Sci. Technol.* **39**(3), 279–281.

Becke A. D. (1993) Density functional thermochemistry. III. The role of exact exchange. *J. Chem. Phys.* **98**(7), 5648–5652.

Besserguenev A., Fogg A., Francis R., Price S., O'hare D., Isupov V. and Tolochko B. (1997) Synthesis and structure of the gibbsite intercalation compounds $[LiAl_2(OH)_6]$ X $\{X = Cl^-, Br^-, NO_3^-\}$ and $[LiAl_2(OH)_6].Cl.H_2O$ using synchrotron x-ray and neutron powder diffraction. *Chem. Mater.* **9**(1), 241–247.

Brenot A., Cloquet C., Vigier N., Carignan J. and France-Lanord C. (2008) Magnesium isotope systematics of the lithologically varied Moselle river basin, France. *Geochim. Cosmochim. Acta* **72**(20), 5070–5089.

Bigeleisen J. and Mayer M. G. (1947) Calculation of equilibrium constants for isotopic exchange reactions. *J. Chem. Phys.* **15**(5), 261–267.

Chan L. H. and Hein J. R. (2007) Lithium contents and isotopic compositions of ferromanganese deposits from the global ocean. *Deep-Sea Res. Part Ii-Topical Stud. Oceanograph.* **54**(11–13), 1147–1162.

Chan L. H., Edmond J. M., Thompson G. and Gillis K. (1992) Lithium isotopic composition of submarine basalts – implications for the lithium cycle in the oceans. *Earth Planet. Sci. Lett.* **108**(1–3), 151–160.

Chan L. H., Edmond J. M. and Thompson G. (1993) A lithium isotope study of hot-springs and metabasalts from midocean ridge hydrothermal systems. *J. Geophys. Res.-Solid Earth* **98**(B6), 9653–9659.

Chan L. H., Gieskes J. M., You C. F. and Edmond J. M. (1994) Lithium isotope geochemistry of sediments and hydrothermal fluids of the Guaymas Basin, Gulf of California. *Geochim. Cosmochim. Acta* **58**(20), 4443–4454.

Colla C. A., Wimpenny J., Yin Q.-Z., Rustad J. R. and Casey W. H. (2013) Calcium-isotope fractionation between solution and solids with six, seven or eight oxygens bound to Ca (II). *Geochim. Cosmochim. Acta* **121**, 363–373.

Fogg A. M. and O'Hare D. (1999) Study of the intercalation of lithium salt in gibbsite using time-resolved in situ X-ray diffraction. *Chem. Mater.* **11**(7), 1771–1775.

Heumann K. G. (1985) Isotopic separation in systems with crown ethers and cryptands. *Org. Chem. Springer*, 77–132.

Hou X. and Kirkpatrick R. J. (2001) Thermal evolution of the Cl-$LiAl_2$ layered double hydroxide: a multinuclear MAS NMR and XRD perspective. *Inorg. Chem.* **40**(25), 6397–6404.

Huh Y., Chan L. H., Zhang L. and Edmond J. M. (1998) Lithium and its isotopes in major world rivers: implications for weathering and the oceanic budget. *Geochim. Cosmochim. Acta* **62**(12), 2039–2051.

Isupov V., Gabuda S., Kozlova S. and Chupakhina L. (1998) Structural mechanism of selective binding of lithium on a solid matrix of $Al(OH)_3$ from aqueous solutions. *J. Struct. Chem.* **39**(3), 362–366.

James R. H. and Palmer M. R. (2000) The lithium isotope composition of international rock standards. *Chem. Geol.* **166**(3), 319–326.

Kim D. (2002) Enrichment of lithium isotopes by a triazacrown trimerrifield peptide resin. *J. Radioanal. Nucl. Chem.* **253**(1), 67–71.

Kim D., Jeon Y., Eom T., Suh M. and Lee C. (1991) Lithium isotope separation on a monobenzo-15-crown-5 resin. *J. Radioanal. Nucl. Chem.* **150**(2), 417–426.

Kim D. W., Jeon Y. S., Jeong Y. K., Suh M. Y. and Joe K. S. (1995) Lithium isotope separation by chemical exchange with polymer-bound azacrown compounds. *J. Radioanal. Nucl. Chem.* **189**(2), 219–227.

Kim D., Hong C. P., Kim C. S., Jeong Y., Jeon Y. S. and Lee J. (1997) Lithium isotope separation on an ion exchange resin having azacrown ether as an anchor group. *J. Radioanal. Nucl. Chem.* **220**(2), 229–231.

Kim D., Kim B., Park S., Lee N., Jeon Y., Choi K. and Lee Y. (1998) Separation of lithium isotope by azacrown tetramerrifield peptide resin. *J. Radioanal. Nucl. Chem.* **232**(1), 257–259.

Kim D., Jang Y., Lee N., Chung Y., Kim K., Park S. and Kim C. (1999) Separation of lithium isotopes by N_4O_2 azacrown ion exchanger. *J. Radioanal. Nucl. Chem.* **240**(1), 155–158.

Kim D., Kim H., Jeon J., Choi K. and Jeon Y. (2000) Separation of lithium isotopes by aminobenzo-15-crown-5 bonded merrifield resin. *J. Radioanal. Nucl. Chem.* **245**(3), 571–574.

Kim D., Kang B., Jeon B. and Jeon Y. (2003) Separation of lithium isotopes by elution chromatography with an AB18C6 bonded Merrifield peptide resin. *J. Radioanal. Nucl. Chem.* **256**(1), 81–85.

Kirkpatrick R. J. (1988) MAS NMR spectroscopy of minerals and glasses. Reviews in mineralogy. *Spectroscop. Meth, Mineral. Geol.* **18**, 341–403, Chapter 9.

Kisakurek B., James R. H. and Harris N. B. W. (2005) Li and delta Li-7 in Himalayan rivers: Proxies for silicate weathering? *Earth Planet. Sci. Lett.* **237**(3–4), 387–401.

Klamt A. and Schüürmann G. (1993) COSMO: a new approach to dielectric screening in solvents with explicit expressions for the screening energy and its gradient. *J. Chem. Soc., Perkin Trans.* **2**(5), 799–805.

Kowalski P. M. and Jahn S. (2011) Prediction of equilibrium Li isotope fractionation between minerals and aqueous solutions at high P and T: an efficient ab initio approach. *Geochim. Cosmochim. Acta* **75**(20), 6112–6123.

Marcus Y. (1988) Ionic radii in aqueous solutions. *Chem. Rev.* **88**(8), 1475–1498.

Massiot D., Fayon F., Capron M., King I., Le Calve S., Alonso B., Durand J. O., Bujoli B., Gan Z. and Hoatson G. (2002) Modelling one- and two- dimensional solid-state NMR spectra. *Magn. Reson. Chem.* **40**(1), 70–76.

Millot R., Vigier N. and Gaillardet J. (2010) Behaviour of lithium and its isotopes during weathering in the Mackenzie Basin. *Canada. Geochimica et Cosmochimica Acta* **74**(14), 3897–3912.

Misra S. and Froelich P. N. (2012) Lithium isotope history of Cenozoic seawater: changes in silicate weathering and reverse weathering. *Science* **335**(6070), 818–823.

Nishizawa K. and Watanabe H. (1986) Intrinsic isotope effect of cryptand (2 b, 2, 1) to li-6 and li-7. *J. Nucl. Sci. Tech.* **23**(9), 843–845.

Nishizawa K. and Takano T. (1988) Extractive separation of lithium isotopes using benzo-15-crown-5. Effect of salt concentration. *Sep. Sci. Technol.* **23**(6–7), 751–757.

Nishizawa K., Ishino S.-I., Watanabe H. and Shinagawa M. (1984a) Lithium isotope separation by liquid–liquid extraction using benzo-15-crown-5. *J. Nucl. Sci. Technol.* **21**(9), 694–701.

Nishizawa K., Watanabe H., Ishino S.-I. and Shinagawa M. (1984b) Lithium isotope separation by cryptand (2B, 2, 1) polymer. *J. Nucl. Sci. Technol.* **21**(2), 133–138.

Nishizawa K., Takano T., Ikeda I. and Okahara M. (1988) Extractive separation of lithium isotopes by crown ethers. *Sep. Sci. Technol.* **23**(4–5), 333–345.

Oi T., Kawada K., Hosoe M. and Kakihana H. (1991) Fractionation of lithium isotopes in cation-exchange chromatography. *Sep. Sci. Technol.* **26**(10–11), 1353–1375.

Ooi K., Miyai Y., Makita Y. and Kanoh H. (1999) Fractionation of lithium isotopes in ion exchange chromatography with titanium phosphate exchanger. *Sep. Sci. Technol.* **34**(6–7), 1133–1144.

Opfergelt S., Georg R., Delvaux B., Cabidoche Y.-M., Burton K. and Halliday A. (2012) Mechanisms of magnesium isotope fractionation in volcanic soil weathering sequences, Guadeloupe. *Earth Planet. Sci. Lett.* **341**, 176–185.

Opfergelt S., Burton K., Georg R., West A., Guicharnaud R., Sigfusson B., Siebert C., Gislason S. and Halliday A. (2014) Magnesium retention on the soil exchange complex controlling Mg isotope variations in soils, soil solutions and vegetation in volcanic soils, Iceland. *Geochim. Cosmochim. Acta* **125**, 110–130.

Otake K., Suzuki T., Kim H.-J., Nomura M. and Fujii Y. (2006) Novel syntheses method of phenol type benzo-15-crown-5 ether resin and its application for lithium isotope separation. *J. Nucl. Sci. Technol.* **43**(4), 419–422.

Pistiner J. S. and Henderson G. M. (2003) Lithium-isotope fractionation during continental weathering processes. *Earth Planet. Sci. Lett.* **214**(1–2), 327–339.

Pogge von Strandmann P. A. E., Opfergelt S., Lai Y. J., Sigfússon B., Gislason S. R. and Burton K. W. (2012) Lithium, magnesium and silicon isotope behaviour accompanying weathering in a basaltic soil and pore water profile in Iceland. *Earth Planet. Sci. Lett.* **339**, 11–23.

Pogge von Strandmann P. A. P., Jenkyns H. C. and Woodfine R. G. (2013) Lithium isotope evidence for enhanced weathering during Oceanic Anoxic Event 2. *Nat. Geosci.* **6**(8), 668–672.

Richens D. T. (1997) *The Chemistry of Aqua Ions: Synthesis, Structure and Reactivity: A Tour Through the Periodic Table of the Elements*. Wiley.

Richter F. M., Mendybaev R. A., Christensen J. N., Hutcheon I. D., Williams R. W., Sturchio N. C. and Beloso A. D. (2006) Kinetic isotopic fractionation during diffusion of ionic species in water. *Geochim. Cosmochim. Acta* **70**(2), 277–289.

Rosenqvist J. and Casey W. H. (2004) The flux of oxygen from the basal surface of gibbsite (α-Al $(OH)_3$) at equilibrium. *Geochim. Cosmochim. Acta* **68**(17), 3547–3555.

Rudnick R. L., Tomascak P. B., Njo H. B. and Gardner L. R. (2004) Extreme lithium isotopic fractionation during continental weathering revealed in saprolites from South Carolina. *Chem. Geol.* **212**(1–2), 45–57.

Rustad J. R., Nelmes S. L., Jackson V. E. and Dixon D. A. (2008) Quantum-chemical calculations of carbon-isotope fractionation in CO_2 (g), aqueous carbonate species, and carbonate minerals. *J. Phys. Chem. A* **112**(3), 542–555.

Rustad J. R., Casey W. H., Yin Q. Z., Bylaska E. J., Felmy A. R., Bogatko S. A., Jackson V. E. and Dixon D. A. (2010) Isotopic fractionation of Mg^{2+} (aq), Ca^{2+} (aq), and Fe^{2+} (aq) with carbonate minerals. *Geochim. Cosmochim. Acta* **74**(22), 6301–6323.

Ryu J.-S., Vigier N., Lee S.-W., Lee K.-S. and Chadwick O. A. (2014) Variation of lithium isotope geochemistry during basalt weathering and secondary mineral transformations in Hawaii. *Geochim. Cosmochim. Acta* **145**, 103–115.

Saalfeld H. and Wedde M. (1974) Refinement of the crystal structure of gibbsite. *Zeitschrift für Kristallographie-Cryst. Mater.* **139**(1–6), 129–135.

Stebbins J. F. (1988) NMR spectroscopy and dynamic processes in mineralogy and geochemistry. reviews in mineralogy. *Spectroscop. Meth. Mineral. Geol.* **18**, 405–429, Chapter 10.

Stebbins J. F. and Xue X. (2014) NMR spectroscopy of inorganic earth materials. *Rev. Mineral. Geochem.* **78**(1), 605–653.

Tarasov K. A., Isupov V. P., Chupakhina L. E. and O'Hare D. (2004) A time resolved, in-situ X-ray diffraction study of the de-intercalation of anions and lithium cations from $[LiAl_2(OH)_6]$ n X· q H_2O ($X = Cl^-$, Br^-, NO_3^-, SO_4^{2-}). *J. Mater. Chem.* **14**(9), 1443–1447.

Taylor T. I. and Urey H. C. (1938) Fractionation of the lithium and potassium isotopes by chemical exchange with zeolites. *J. Chem. Phys.* **6**(8), 429–438.

Teng F. Z., McDonough W. F., Rudnick R. L., Dalpe C., Tomascak P. B., Chappell B. W. and Gao S. (2004) Lithium isotopic composition and concentration of the upper continental crust. *Geochim. Cosmochim. Acta* **68**(20), 4167–4178.

Urey H. C. (1947) The thermodynamic properties of isotopic substances. *J. Chem. Soc.*, 562–581.

Verney-Carron A., Vigier N. and Millot R. (2011) Experimental determination of the role of diffusion on Li isotope fractionation during basaltic glass weathering. *Geochim. Cosmochim. Acta* **75**(12), 3452–3468.

Vigier N., Decarreau A., Millot R., Carignan J., Petit S. and France-Lanord C. (2008) Quantifying Li isotope fractionation during smectite formation and implications for the Li cycle. *Geochim. Cosmochim. Acta* **72**(3), 780–792.

Wang S.-L., Cheng C.-Y., Tzou Y.-M., Liaw R.-B., Chang T.-W. and Chen J.-H. (2007) Phosphate removal from water using lithium intercalated gibbsite. *J. Hazard. Mater.* **147**(1), 205–212.

Williams L. B. and Hervig R. L. (2005) Lithium and boron isotopes in illite-smectite: the importance of crystal size. *Geochim. Cosmochim. Acta* **69**(24), 5705–5716.

Williams G. R. and O'Hare D. (2006) A kinetic study of the intercalation of lithium salts into $Al(OH)_3$. *J. Phys. Chem. B* **110**(22), 10619–10629.

Wimpenny J., Gíslason S., James R. H., Gannoun A., Pogge von Strandmann P. A. E. and Burton K. W. (2010a) The behaviour of Li and Mg isotopes during primary phase dissolution and secondary mineral formation in basalt. *Geochim. Cosmochim. Acta* **74**(18), 5259–5279.

Wimpenny J., James R., Burton K., Gannoun A., Mokadem F. and Gíslason S. (2010b) Glacial effects on weathering processes: new insights from the elemental and lithium isotopic composition of West Greenland rivers. *Earth Planet. Sci. Lett.* **290**(3–4), 427–437.

Wimpenny J., Colla C. A., Yin Q.-Z., Rustad J. R. and Casey W. H. (2014) Investigating the behaviour of Mg isotopes during the formation of clay minerals. *Geochim. Cosmochim. Acta* **128**, 178–194.

Wunder B., Meixner A., Romer R. L. and Heinrich W. (2006) Temperature-dependent isotopic fractionation of lithium between clinopyroxene and high-pressure hydrous fluids. *Contrib. Miner. Petrol.* **151**(1), 112–120.

Wunder B., Meixner A., Romer R. L., Feenstra A., Schettler G. and Heinrich W. (2007) Lithium isotope fractionation between Li-bearing staurolite, Li-mica and aqueous fluids: an experimental study. *Chem. Geol.* **238**(3), 277–290.

Yamaji K., Makita Y., Watanabe H., Sonoda A., Kanoh H., Hirotsu T. and Ooi K. (2001) Theoretical estimation of lithium isotopic reduced partition function ratio for lithium ions in aqueous solution. *J. Phys. Chem. A* **105**(3), 602–613.

Zhang L. B., Chan L. H. and Gieskes J. M. (1998) Lithium isotope geochemistry of pore waters from Ocean Drilling Program Sites 918 and 919, Irminger Basin. *Geochimica Et Cosmochimica Acta* **62**(14), 2437–2450.

Associate editor: Fang-Zhen Teng